Published in Journal of Hydrology, 266, issues 1-2, 99-119, 2002
which should be used for any reference to this work

Flow behavior in a dual fracture network

Hervé Jourde[a,*], Fabien Cornaton[b], Séverin Pistre[a], Pascal Bidaux[a,1]

[a]*Laboratoire Hydrosciences, ISTEEM, UMR 5569 du CNRS, Montpellier II University, Place E. Bataillon, 34095 Montpellier Cedex 5, France*
[b]*CHYN, University of Neuchâtel, Rue Emile-Argand 11, CH-2007 Neuchâtel, Switzerland*

Abstract

A model that incorporates a pseudo-random process controlled by mechanical rules of fracturing is used to generate 3D orthogonal joint networks in tabular stratified aquifers. The results presented here assume that two sets of fractures, each with different conductivities, coexist. This is the case in many aquifers or petroleum reservoirs that contain sets of fractures with distinct hydraulic properties related to each direction of fracturing. Constant rate pump-tests from partially penetrating wells are simulated in synthetic networks. The transient head response is analyzed using the type curve approach and plots, as a function of time, of pressure propagation in the synthetic network are shown. The hydrodynamic response can result in a pressure transient that is similar to a dual-porosity behavior, even though such an assumption was not made a priori. We show in this paper that this dual porosity like flow behavior is, in fact, related to the major role of the network connectivity, especially around the well, and to the aperture contrast between the different families of fractures that especially affects the earlier hydrodynamic response. Flow characteristics that may be interpreted as a dual porosity flow behavior are thus related to a lateral heterogeneity (large fracture or small fault). Accordingly, when a dual porosity model matches well test data, the resulting reservoir parameters can be erroneous because of the model assumptions basis that are not necessarily verified. Finally, it is shown both on simulated data and well test data that such confusion in the interpretation of the flow behavior can easily occur. Well test data from a single well must therefore be used cautiously to assess the flow properties of fractured reservoirs with lateral heterogeneities such as large fractures or small faults.

Keywords: Fractured reservoir; Pumping tests; Pressure transient response; Dual porosity behavior; Heterogeneity; Connectivity

1. Introduction

The hydraulic properties of fractured reservoirs are of great importance to the management of groundwater and petroleum resources. Fluid flow related to connected networks of fractures can influence the migration of water-soluble wastes and the distribution of petroleum accumulations. At the scale of the Earth's crust, fractures are very frequent tectonic elements. The most common fracture pattern is composed of two sets of orthogonal joints perpendicular to the strata. Such fracture systems have been characterized in the field (Pollard and Aydin, 1988; Huang and Angelier, 1989; Rives et al., 1994) and reproduced in experiments (Rives et al., 1994; Wu and Pollard, 1995). Observations made at different scales have shown that network patterns are not random, but rather are controlled by mechanical interactions between joints during network genesis, which

* Corresponding author. Fax: +33-4671-44-774.
E-mail address: herve.jourde@msem.univ-montp2.fr (H. Jourde).
[1] PERENCO SA 23-25, rue Dumond Durville, 75116 Paris, France.

Nomenclature

(ij)	indices referring to element joining nodes (i) and (j)
L_{ij}	length of an element (ij)
k_{ij}	integrated hydraulic conductivity of an element (ij)
S_{ij}	integrated storativity of an element (ij)
x_{ij}	abscissa along the element (ij)
h_0	initial head in the aquifer
h_{ij}	hydraulic head between nodes i and j
$\partial h_{ij}/\partial x_{ij}$	hydraulic gradient between nodes i and j
q_{ij}	flow rate through an element (ij)
μ	kinematic viscosity
g	gravity constant
$\mathrm{d}V$	elementary volume
β	elastic constant
r	distance between a piezometer node and the pumping node
rd	dimensionless distance between a piezometer node and the pumping node
T	thickness of the synthetic network
th	average thickness of the strata and length unit
$\hat{K}_\mathrm{h}$	equivalent horizontal conductivity of the synthetic network
$\hat{S}_\mathrm{s}$	equivalent specific storativity of the synthetic network.
$\hat{D}_\mathrm{h}$	equivalent diffusivity of the synthetic network $= \hat{K}_\mathrm{h}/\hat{S}_\mathrm{s}$
Q	flow rate at the pumping well.
s_d	dimensionless drawdown $= (2\pi\hat{K}_\mathrm{h}T/Q)s$
t	time
t_d	dimensionless time $= \hat{D}_\mathrm{h}t/\mathrm{th}^2$
p	Laplace parameter
$\bar{s}_{ij}$	drawdown along the element ij in Laplace domain
$\bar{s}_i$	drawdown at node i in Laplace domain
$\bar{s}_j$	drawdown at node j in Laplace domain
$\bar{q}_i(p)$	flow rate at node i in Laplace domain

explains statistical properties (length, spacing, density, aspect ratio, etc.) and affects network connectivity.

In the fracture network model considered in this study, simple mechanical rules of fracturing are taken into account in an algorithm that uses a pseudo-random process to generate orthogonal fracture sets in a stratified aquifer. This model is proposed to simulate synthetic fracture network in layered rocks and the pressure transient response induced by pumping test (Jourde et al., 1998). The hydrodynamic behavior of the synthetic reservoir is studied by considering a pump-test of a single-phase fluid from a well that partially penetrates the simulated network. It is assumed that flow occurs at intersections between discontinuities, fractures, or bedding parallel joints, which are modeled as pipes with various dimensions.

Common testing methods examine the change of fluid pressure in a well while it is being produced at a constant rate (drawdown test) or shutin after a prolonged production period (buildup test). Fluid flow properties of fracture networks can thus be estimated from transient well testing (Warren and Root, 1963; Gringarten et al., 1974; Bourdet et al., 1983; Horne, 1995; Hamm and Bidaux, 1996). One must notice that the interpretation of pressure test data is not an easy task, especially for fractured reservoirs in which the connectivity of the flow paths network as

well as the hydraulic properties of the different features are usually unknown and may induce particular flow behavior. In this paper, the transient flow response is analyzed by using the derivative of the drawdown with time multiplied by time (Bourdet et al., 1983) and the approximation of the generalized radial flow model (Barker, 1988). The pressure transient response was found to be very sensitive to both the connectivity around the well and the aperture contrast between the different families of fracture that together can induce a dual porosity-like behavior.

The paper is organized as follows: First, we describe how we simulate fracture networks and transient well tests. We present results of simulations while varying hydrodynamic properties of the network. We then investigate what is the origin of this dual porosity-like pressure transient response in the synthetic networks representative of natural fractured reservoir. We show that this behavior is related to a connectivity that differs from the assumptions usually considered for dual porosity model and how it is sensitive to the different hydrodynamic properties of the network. With the example of a fractured reservoir with identical properties as the modeled network, we finally show that well test data interpreted as dual porosity could also correspond to a flow behavior related to a lateral heterogeneity made of a large fracture in the vicinity of the well. We conclude with a discussion of well test interpretations that are informed by our new results.

2. Three dimensional fracture network model

As this is not the focus of this paper, we will not give an extended explanation about the model, but simply remind the reader about the main assumptions.

The model allows the simulation of a network constituted of two orthogonal generations of joints in a tabular stratified medium (Fig. 1). Orthogonal joints perpendicular to bedding constitute one of the most common patterns of joints found on superficial outcrops of sedimentary rocks and occur in many oil reservoirs and aquifer in sedimentary terrain. Abutting and crosscutting relationships as well as markedly differing joint orientations seem to imply that the two sets formed neither at the same time nor under the same stress conditions (Bai and Gross, 1999). In our model, we consider that the second set of fractures is younger than the first set. We focus on partially crosscutting patterns in which the first joint set has the longest fractures that are abutted or crosscut by the second set. The development of a fracture produces stress relaxation in its vicinity (Segall and Pollard, 1983). This relaxation zone affects a small zone around each fracture in which no new fracture can form (Rives et al., 1994; Becker and Gross, 1996). This zone of reduced stress, referred to as the stress reduction shadow or *shadow zone*, scales with joint heights and is responsible for the observed correlation between joint spacing and bed thickness (Hobbs, 1967; Price and Cosgrove, 1990). The distribution of spacing between joints of the same set is negative exponential at the earliest stage of joint development, then log-normal, and finally becomes normal when the rock layer is *saturated* (Rives et al., 1994; Wu and Pollard, 1995).

Accordingly, the pseudo-random approach, considered for joint generation and propagation in our model, is based on the following simple mechanical descriptions of fracture propagations and mechanical interactions:

- A random process gives the thickness of the strata according to a log−normal distribution;
- The joints of the first and second generations grow from randomly distributed flaws (uniform distribution);
- The joints are controlled by the concept of a shadow zone and *rock layer saturation*;
- Second generation joints cross or abut those of the first generation;
- The joints can cross-cut some strata but will always be bounded by a stratum interface;
- The joints have a rectangular shape.

The synthetic patterns obtained give good results from a visual standpoint as well as from a statistical standpoint approach (Jourde et al., 1998; Jourde, 1999). Indeed, the match between synthetic networks and different outcrops were demonstrated by various statistical analyses. The spacing of the first generation joints in the different layers follows a normal distribution, as it should in saturated strata. The

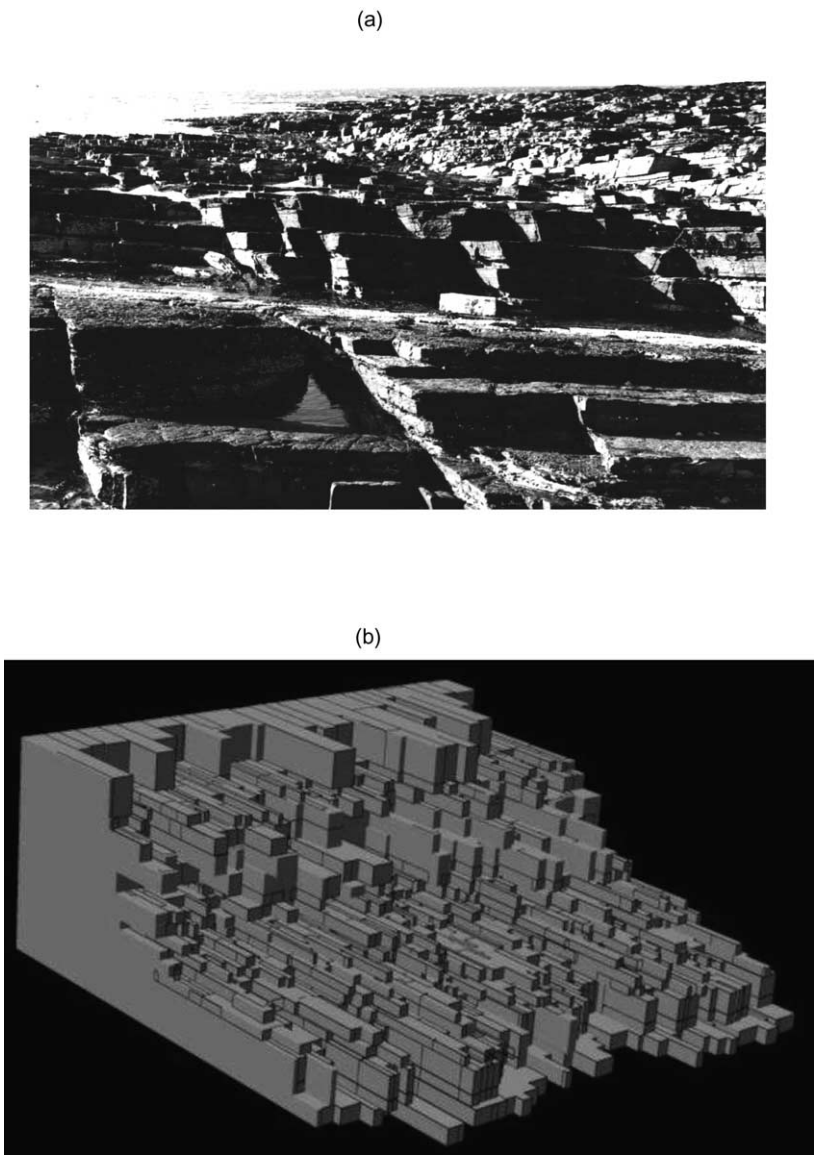

Fig. 1. Orthogonal joint network; (a) Natural example of Devonian sandstone (average thickness of individual layers = 50 cm), Scotland (photo V. Auzias); (b) Simulated example.

length distribution, after all the horizontal interactions between fractures, remains lognormal, which is in agreement with field observations in layered fractured rocks. The relationship between average joint spacing and bed thickness is determined stratum by stratum and is nearly linear, which is also a characteristic of sedimentary rocks (Huang and Angelier, 1989; Wu and Pollard, 1995).

3. Transient flow model

In flow models for fractured networks, it is generally assumed that flow is diffuse (between plate) or homogeneously channelized within each fracture. However, observations of the channelization of flow in conduits at intersections between fractures suggest that intersections may be more important flow

paths, especially in stratified sedimentary rocks (Drogue and Grillot, 1976; Sanderson and Zhang, 1997; Bruel et al., 1999; Cornaton and Perrochet, 2002).

In limestone, Drogue and Grillot (1976) have shown direct evidence of flow at the intersection between fractures and bedding-parallel planes by temperature and flow-meter measurement. These authors also identified channeling at these intersections with video logging. Irrespective of the reservoir rock and the intersection shape, mineralization is expected to begin away from the intersection, where the aperture is narrow. Over time, such mineralization increasingly concentrates flow at the intersections, which remain the most important channels until complete infilling of the system (Drogue and Costa Almeida, 1984). Sanderson and Zhang (1997) demonstrated that a change in the stress state might open up pipes at fracture intersections and result in a sudden transition from diffuse flow through fracture networks to highly localized flow. This may be the case in many aquifers, where pumping or changes in the regional stress field change the stress state and create such channelized flow in pipes. Such channeling has also been identified in deep mines (Bruel et al., 1999) and the pumping test data presented hereafter come from a field site where flow matches this particular case.

Accordingly, the stratified fractured reservoir can be described as a system composed of pipes linking nodes in which pipes correspond to intersections between fractures or between fracture and bedding plane. A sub-horizontal channel (pipe) is generated when a sub-vertical joint intersects a low dip and flat bedding plane. A sub-vertical channel (pipe) is generated when two joints of different sets intersect each other. In such layered fractured rocks, two types of intersections can be considered: (1) T-shape intersections which occur when a joint of the second set abuts a joint of the first set, or when a joint abuts a bedding plane; and (2) X-shape intersections which occur when a joint of the second set crosscuts a joint of the first set, or when a joint crosses a bedding plane.

In the present study, we consider a reservoir whose matrix is impermeable and constituted of non-karstic sedimentary rocks. In this case, the T-shape intersection between second-set joints and first set joints may have a larger aperture than X-shape intersections (Fig. 2). Indeed, in T-shape intersections, the first set joint has an aperture large enough to create a free surface effect, such that the second set joint abuts the first set joint. In X-shape intersections, the first set joint must be close enough for a local contact across the first-set joint where the second set joint crosscuts. Hence, flow paths are likely to have lower aperture along X-shape intersections than along T-shape intersections in such fractured reservoirs (Bruel et al., 1999).

The aperture of preferred flow paths (pipe diameter) is chosen on the basis of the type of intersection (T-shape or X-shape) and the lithology of the matrix. Radii of horizontal pipes formed by intersections of second set joints with bedding planes are always ‘small’ (Fig. 2). Assignment of pipe radii as a function of joint orientation enables accounting for hydraulic properties anisotropy, as is observed in many layered fractured systems (Barthélémy et al., 1996). This anisotropy reflects the fact that a set of joints may be hydraulically less efficient for various reasons such as the regional or local state of stress, the continuity of the fracture set, or the connectivity of the network.

For the simulation of pressure transient responses, we therefore consider a pipe network model representative of flow paths in the fracture network with the following assumptions:

- Flow in the matrix as well as in fracture plane is neglected;
- The permeable network is composed of mono-dimensional elements (pipes) that correspond to intersections between fractures or between fracture and bedding plane. Different hydraulic properties can be affected to pipes according to intersections type and reservoir properties (Jourde et al., 1998; Jourde, 1999);
- Flow in the pipes is laminar (Poiseuille flow);
- The aquifer is confined with no-flux boundary conditions imposed at the sides of the pattern.

One large connective cluster of pipes is generally obtained. Then, the pump-test is modeled while considering a well producing at a constant rate and partially penetrating the connective cluster. Fluid flow in this discrete system is simulated by the traditional mass conservation approach, which allows a good resolution of the earlier data.

Flow is thus computed by applying the diffusivity

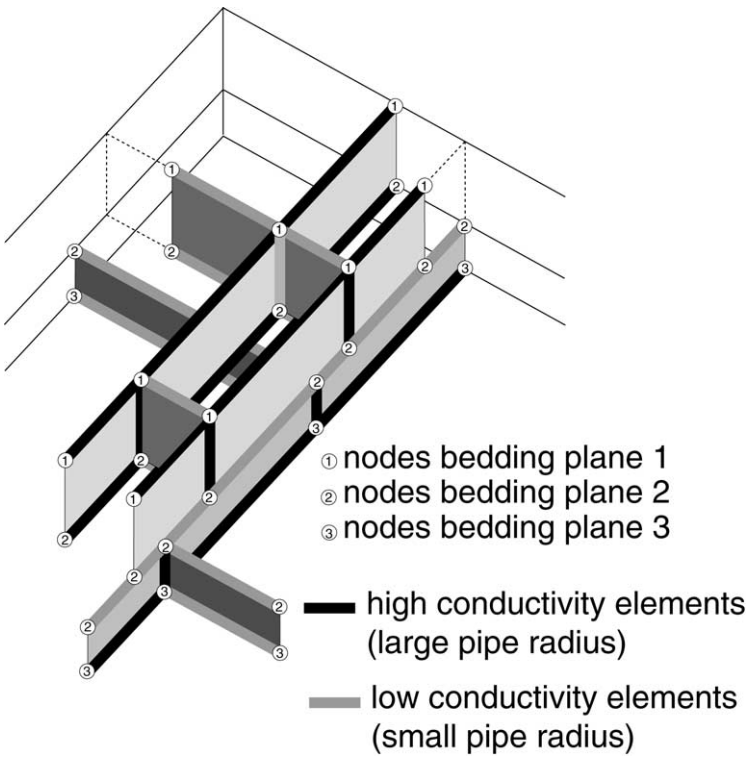

Fig. 2. Assignment of preferred flow paths aperture (pipe diameter) on the basis of the type of intersection. T-shape intersections have larger aperture than X-shape intersections for pipes belonging to first set joints. Horizontal pipes formed by intersections of second set joints with bedding planes are always 'small'.

equation to each pipe, and the principle of continuity and mass conservation at nodes, assuming that nodes are not capacitive.

The diffusivity equation, written in terms of the hydraulic head h_{ij} measured along pipe (ij) of length L_{ij} [L] joining nodes (i) and (j), is:

$$\frac{k_{ij}}{S_{ij}}\frac{\partial^2 h_{ij}}{\partial x_{ij}^2} = \frac{\partial h_{ij}}{\partial t} \tag{1}$$

with k_{ij} and S_{ij}, the integrated hydraulic conductivity [L^3T^{-1}] and integrated storativity [L] of pipe (ij), respectively, x_{ij} the abscissa along pipe (ij) $(0 < x_{ij} < L_{ij})$. By definition (Cacas et al., 1990), k_{ij} is the ratio between the flow rate q_{ij} through a pipe (ij) and the hydraulic head gradient in the pipe:

$$q_{ij} = -k_{ij}\frac{\partial h_{ij}}{\partial x_{ij}} \tag{2}$$

$$k_{ij} = (\pi g/8\mu)R^4 \tag{3}$$

where μ [L^2T^{-1}] is the kinematic viscosity of the fluid and R [L] is the radius of the pipe.

Throughout this paper, the *integrated hydraulic conductivity* will be referred as *conductivity* for easier writing.

By analogy, we defined the integrated storativity of an element S_{ij} as the volume of fluid released per length unit of the element for a unit change in hydraulic head (Jourde et al., 1998):

$$\frac{\partial q_{ij}}{\partial x_{ij}} = -S_{ij}\frac{\partial h_{ij}}{\partial t} \tag{4}$$

$$S_{ij} = \beta\pi R^2 \tag{5}$$

where $\beta = B_f + C_w$ [1/L] is an elastic constant that accounts for both the compressibility of the fracture (B_f) and the fluid (C_w), assuming the matrix compressibility negligible.

Considering now the principle of continuity at

node (i), it can be written as:

$$h_{ij}(x_{ij}=0,t)=h_{ik}(x_{ik}=0,t)=h_i(t) \tag{6}$$

with h_i (t) the hydraulic head at node (i) and time t.

Introducing the diffusivity of an element $D_{ij}=k_{ij}/S_{ij}$, Eq. (1) can be written as:

$$D_{ij}\frac{\partial^2 h_{ij}}{\partial x_{ij}^2}=\frac{\partial h_{ij}}{\partial t} \tag{7}$$

For convenience, the diffusivity equation is written in terms of drawdown rather than head. Drawdown s_{ij} is defined as $s_{ij}=h_0-h_{ij}$, where h_0 is the initial head; the diffusivity Eq. (7) becomes:

$$D_{ij}\frac{\partial^2 s_{ij}}{\partial x_{ij}^2}=\frac{\partial s_{ij}}{\partial t} \tag{8}$$

Finally, mass conservation at nodes assuming that nodes are not capacitive gives:

$$\sum_{i\neq j}k_{ij}\left(\frac{\partial s_{ij}}{\partial x_{ij}}\right)_{x_{ij}=0}=q_i(t) \tag{9}$$

where q_i (t) is the flow rate withdrawn from the reservoir at node i and time t. Assuming that the pumping well (node w) produces at a constant rate Q, this implies q_w (t) $=Q$ at node w and q_i (t) $=0$ elsewhere.

Barker (1991) established steady flow equations for pipe networks. In order to solve the problem in transient-state, Ezzedine (1994) took the same approach using an analogy to the steady-state problem in the Laplace domain. Thus, following the procedure devised by this author, the use of Laplace transforms in each element leads to an ordinary differential equation:

$$D_{ij}\frac{\mathrm{d}^2\bar{s}_{ij}}{\mathrm{d}x_{ij}^2}=p\bar{s}_{ij} \tag{10}$$

where p denotes the Laplace parameter and $\bar{s}_{ij}$ is the p-transformed drawdown along the element ij, of length L_{ij}, in Laplace domain. This formulation allows us to express

$$\left(\frac{\mathrm{d}\bar{s}_{ij}}{\mathrm{d}x_{ij}}\right)_{x_{ij}=0}$$

linearly as a function of $\bar{s}_i=\bar{s}_{ij}(x_{ij}=0)$ and $\bar{s}_j=\bar{s}_{ij}(x_{ij}=L_{ij})$, and hence to write the Kirschoff equations in terms of $\bar{s}_i$ and $\bar{s}_j$ without derivatives. Therefore, the analytic solution of Eq. (10) (Ezzedine, 1994) reads:

$$\bar{s}_{ij}(x,p)=\bar{s}_i(p)\cosh(\lambda_{ij}x)+\frac{\sinh(\lambda_{ij}x)}{\sinh(\lambda_{ij}L_{ij})}(\bar{s}_j(p)-\bar{s}_i(p)\cosh(\lambda_{ij}L_{ij})) \tag{11}$$

with

$$\lambda_{ij}^2=\frac{p}{D_{ij}}.$$

Taking the derivative of Eq. (11) and substituting it into Eq. (9) we obtain:

$$\sum_j -\frac{k_{ij}\lambda_{ij}}{\sinh(\lambda_{ij}L_{ij})}[s_j(p)-\bar{s}_i(p)\cosh(\lambda_{ij}L_{ij})]=\bar{q}_i(p) \tag{12}$$

where $\bar{q}_i(p)=Q/p$ at the point sink and $\bar{q}_i(p)=0$ elsewhere. That is, for any value of the Laplace variable p, the drawdown at the N nodes is calculated by solving a linear system of N equations:

$$\sum_j a_{ij}\bar{s}_j(p)=\bar{q}_i(p) \tag{13}$$

with

$$a_{ij}=-\frac{k_{ij}\lambda_{ij}}{\sinh(\lambda_{ij}L_{ij})},\quad i\neq j;\ \text{and}\ a_{ii}=\sum_{j\neq i}k_{ij}\lambda_{ij}\coth(\lambda_{ij}L_{ij}).$$

Finally, the real drawdown s is computed from $\bar{s}$ by a numerical inverse Laplace transform (Stehfest, 1970).

4. Transient flow behavior in the synthetic network

Pump-test simulations can be carried out at a constant rate on a node situated at a stratigraphic interface (Jourde et al., 1998), which corresponds to the ideal case of an experimental site in which the well is equipped with packers that isolate all permeable levels. In order to represent more realistic near-wellbore geometry, we consider here a well that penetrates a finite thickness of the formation (Fig. 3(a)). All of the elements intersected by a cylinder of defined radius and height (corresponding to the well)

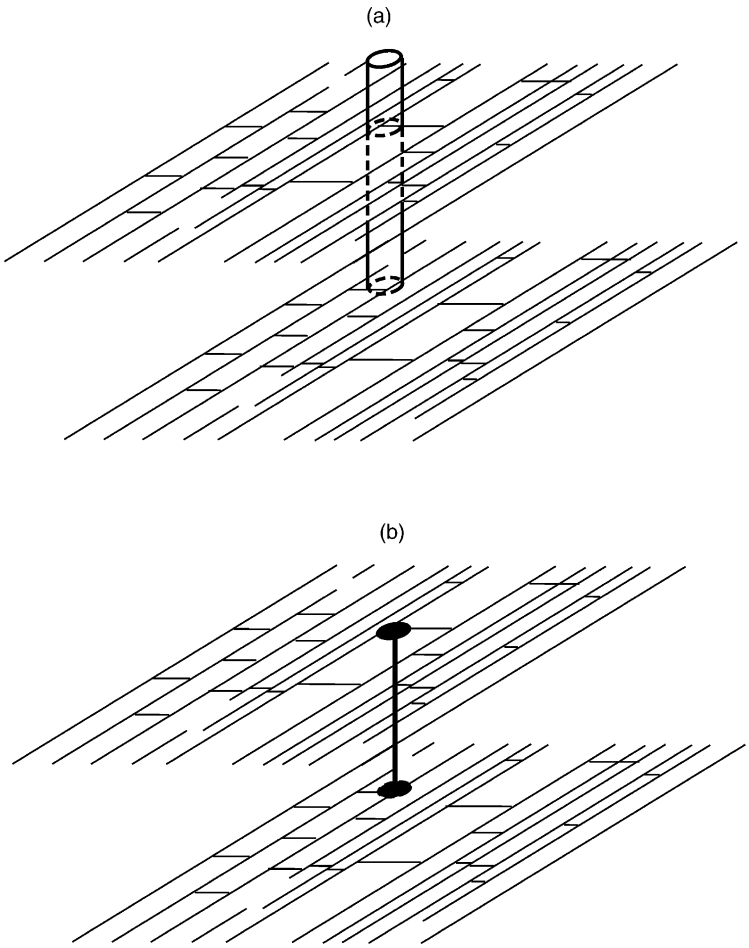

Fig. 3. Representation of a well partially penetrating the synthetic network (only the pipes situated on bedding parallel-planes are shown); (a) a cylinder of defined radius and height represents the well; (b) the well is numerically considered as a unique node (represented in the two bedding parallel plane in this scheme), that is connected to all the elements intersected by the previous cylinder. It is virtually present in all the strata containing an intersected element and corresponds to a well without wellbore storage.

are connected to one unique node virtually present in all layers intersected by the well (Fig. 3(b)). The hydraulic head calculated on this node represents the head that would be measured on a well of infinite conductivity (without wellbore storage).

The simulated pressure transient response is then represented for different wells and different network characteristics, using the dimensionless parameters defined as follows:

- $r_d = r/\mathrm{th}$, the dimensionless distance between an observation well (node) and the pumping well and r the Euclidean distance between the latter; $\mathrm{th} = T/n$ (L) is the average thickness of the n strata constituting the synthetic network of thickness T;
- $s_d = (2\pi\hat{K}_h T/Q)s$, the dimensionless drawdown where $\hat{K}_h$ [LT^{-1}] is the equivalent horizontal conductivity of the synthetic network, Q [L^3T^{-1}] is the flow rate and s is the drawdown at the pumping well.
- $t_d = \hat{D}_h t/\mathrm{th}^2$ with $\hat{D}_h = \hat{K}_h/\hat{S}_s$ [L^2T^{-1}] the equivalent diffusivity, and $\hat{S}_s$ [L^{-1}] the equivalent specific storage of the synthetic network.

In most pumping test simulations, when the whole network is queried (i.e, for large t_d), the observed flow

behavior is radial. This is why we chose the preceding dimensionless drawdown. For the same reason, the equivalent horizontal conductivity is defined as $\hat{K}_h = \sqrt{K_x K_y}$, with K_x [LT^{-1}] and K_y [LT^{-1}] being the equivalent conductivities along the x and y axes, respectively. K_x and K_y are calculated by considering several cross-sections (more than 100 in general) of the synthetic network, respectively, orthogonal to x- and y-directions. For each cross-section, we determine $n1$ (the number of pipes of small radius ($r1$) per surface unit) and $n2$ (the number of pipes of high radius ($r2$) per surface unit) in order to calculate the mean values of these parameters referred as $mn1$ [L^{-2}] and $mn2$ [L^{-2}], respectively (with subscript x or y depending on the direction considered). If we denote $k1$ [L^3T^{-1}] and $k2$ [L^3T^{-1}] as the respective pipe conductivity of element of radius $r1$ and $r2$, then:

$$K_x = mn1_x\, k1 + mn2_x\, k2; \text{ and}$$

$$K_y = mn1_y\, k1 + mn2_y\, k2$$

The equivalent specific storativity S is calculated by considering $l1$ [L^{-2}] and $l2$ [L^{-2}] as the total length of pipes of small ($r1$) and high ($r2$) radius per volume unit in the whole network, respectively. If we make $S1$ [L] and $S2$ [L] the pipe storage (integrated storativity) of elements of radius $r1$ and $r2$, respectively, then:

$$S = l1\, S1 + l2\, S2$$

The dimensionless drawdown s_d and the derivative $ds_d/d\log(t_d)$ which reflects the dimensionless rate of pressure change with time multiplied by time (Bourdet et al., 1983) are plotted in logarithmic coordinates as a function of dimensionless time t_d at the pumping well or t_d/r_d^2 at an observation well.

The simulated curves are interpreted using an approximation of the generalized radial flow model of Barker (1988). This author proposed a model by considering a generalized diffusivity equation involving fractional dimension. This generalized radial flow (GRF) model generalizes the flow dimension to non-integral values, while retaining the assumptions of radial flow and homogeneity of the fractured medium (hydraulic conductivity K_f and specific storage S_{sf}). It is assumed that the fluid is injected into a source that is an n-dimensional sphere of radius r_w and storage capacity S_w. The source has an infinitesimal skin and defines a surface of exchange that corresponds to the projection of the n-dimensional sphere through three-dimensional space by an amount b^{3-n}. This surface is $\alpha_n r_w^{n-1} b^{3-n}$, with b^{3-n} the lateral extent of the flow region in n dimension. If $n = 2$ the flow is radial and b^{3-n} corresponds to the thickness of the reservoir b. α_n is the area of the unit sphere in n dimensions:

$$\alpha_n = 2\pi^{n/2}/\Gamma(n/2) \tag{14}$$

where $\Gamma(x)$ is the Gamma function.

Considering the above hypothesis and a constant rate of production Q_0, the diffusivity equation is formulated and a solution is given in the Laplace domain. Then, after inversion of the equation to real domain, the drawdown $s(r,t)$ in the fracture system can be expressed as a function of r, the distance measured in the fractured flow system from the center of source, and time t:

$$s(r,t) = \frac{Q_0 r^{2\nu}}{4\pi^{1-\nu} K_f b^{3-n}} \Gamma(-\nu, u) \qquad \nu < 1 \tag{15}$$

where

$$\nu = 1 - n/2 \tag{16}$$

$$u = S_{sf} r^2 / 4K_f t \tag{17}$$

Eq. (15) is a generalization of the equation given by Theis (1935) for radial flow with a line source. For small values of u (either at the source for small r, or anywhere else for large t), Eq. (15) can be approximate by the asymptotic form:

$$s(r,t) = \frac{Q_0 r^{2\nu}}{4\pi^{1-\nu} K_f b^{3-n} \nu} \left[\left(\frac{4K_f t}{S_{sf}} \right)^{\nu} - \Gamma(1-\nu) r^{2\nu} \right] \tag{18}$$

where $\Gamma(x,y)$ is the incomplete Gamma function and $\nu \neq 0$ ($n \neq 2$).

For a given distance r, Eq. (18) that is a generalization of the Jacob equation (1946) can thus be written as:

$$s(t) = At^{\nu} - B \tag{19}$$

At late time (large t) or at the producing well (small r), the log–log plot of pressure derivative ($dp/d\log(t)$) versus time will yield a straight line with slope $\nu = 1 - n/2$. Eq. (19) can thus be considered as a diagnostic tool to determine the flow dimension

equal to the dimension n of the source, by considering:

$$\nu = 1 - n/2 \tag{20}$$

For the following simulations, the hydraulic properties are calculated while considering water at 20 °C with kinematic viscosity $\mu = 1.003 \times 10^{-6}\ \mathrm{m^2/s}$ and compressibility coefficient $C_w = 4.8 \times 10^{-6}\ \mathrm{m^{-1}}$. For a fissured rock, the compressibility coefficient B_f varies between $7 \times 10^{-6}\ \mathrm{m^{-1}}$ and $3 \times 10^{-6}\ \mathrm{m^{-1}}$ (Domenico and Schwartz, 1990). Accordingly, we choose the elastic constant $\beta = B_\mathrm{f} + C_w$ such as $\beta = 10^{-5}\ \mathrm{m^{-1}}$ to estimate the storativity of each element and the equivalent specific storativity of the whole network.

4.1. Transient well test signatures obtained from pumping-test simulation

Pumping test simulations were carried out on the network shown on Fig. 1(b), the equivalent aperture of the various channels (pipes) constituting the network being, respectively, 0.001 and 0.002 m. While considering the parameters β and μ stated above, this confers to the network the following hydraulic properties:

$$\hat{K}_\mathrm{h} = 1.3 \times 10^{-6}\ \mathrm{m\ s^{-1}};\ \hat{S}_\mathrm{s} = 1.2 \times 10^{-6}\ \mathrm{m^{-1}};$$

$$\hat{D}_\mathrm{h} = 1.08.$$

Fig. 4 shows the transient flow response on a pumping well of equivalent radius 0.2 m, and a penetration ratio of a quarter of the aquifer thickness; it intersects a pipe related to a second-generation fracture in the proximity of a long fracture of first generation (Fig. 5). The hydrodynamic response analyzed with the derivative might be interpreted as a dual porosity behavior, which is followed by a quasi-radial flow ($n = 1.92$).

The dual porosity behavior corresponds to pressure transients in reservoirs that have distinct primary and secondary porosity. These pressure effects are quite commonly seen in naturally fractured reservoirs. In a dual porosity reservoir, a porous 'matrix' of lower transmissivity (primary porosity) is adjacent to higher transmissivity medium (secondary porosity). Dual porosity model are based on the hypothesis that the well intersects the secondary porosity (continuum fracture) which itself drains the primary porosity (continuum matrix).

As described by Gringarten et al. (1974), it is possible to define the fracture system (secondary porosity) hydraulic conductivity as

$$k_\mathrm{f} = k'_\mathrm{f} V_\mathrm{f}$$

and the block system (primary porosity) hydraulic conductivity as

$$k_\mathrm{m} = k'_\mathrm{m} V_\mathrm{m}$$

where k'_f and k'_m are the hydraulic conductivities of representative fissures and matrix rock, respectively, V_f is the ratio of the total volume of the fissures to the bulk volume of the rock mass (the sum of the volume of the fissures and the volume of the matrix), and V_m is the ratio of the total volume of the matrix rocks to the bulk volume. V_f and V_m sum to unity.

In like manner, specific storage of the fissure system can be defined as

$$S_\mathrm{f} = S'_\mathrm{f} V_\mathrm{f}$$

and the specific storage of the blocks can be defined as

$$S_\mathrm{m} = S'_\mathrm{m} V_\mathrm{m}$$

where S'_f and S'_m are the specific storages of representative fissures and matrix rock, respectively.

The main hydraulic parameters specific to dual porosity model to match well test data are the transmissivity ratio and the storativity ratio.

The first of the two parameters is the transmissivity ratio

$$\lambda = \chi k_\mathrm{m} / k_\mathrm{f}\ r_\mathrm{w}^2$$

where r_w is the radius at the production well and χ is a factor that depends on the geometry of the interporosity flow between the matrix and the fractures (Horne, 1995):

$$\chi = \mathrm{SA}/lV$$

where SA is the surface area of the matrix block, V is the matrix volume, and l is a characteristic length that depends on the shape of the matrix blocks.

The second parameter is the storativity ratio ω, that relates the secondary (or fracture) storativity to that of the entire system:

$$\omega = S_\mathrm{f}/(S_\mathrm{f} + S_\mathrm{m})$$

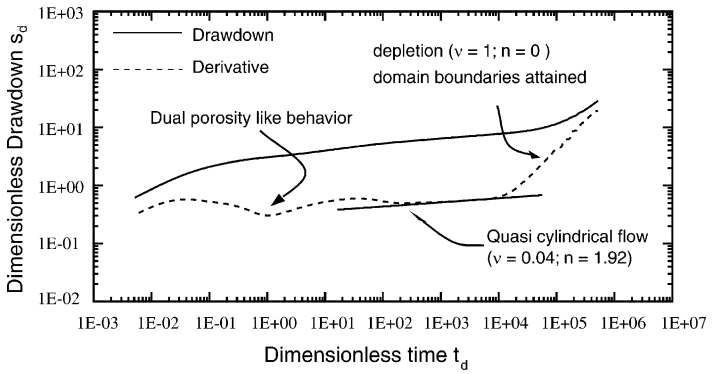

Fig. 4. Hydrodynamic response and transient-well-test signature on the pumping well when the equivalent apertures of the pipes are, respectively, 0.001 and 0.002 m.

In such a dual porosity model, fluid flows to the wellbore through the fracture alone, although may feed from the matrix block (Horne, 1995). Due to the two separate 'porosities' in the reservoir, the dual porosity system has a response that may show characteristics of both of them. The secondary porosity (fractures), having the greater transmissivity and being connected to the wellbore, respond first. The primary porosity does not flow directly into the wellbore and is of lower transmissivity, therefore responds much later. As the pressure change in terms of time is more meaningful than the pressure itself, this behavior is clearly seen when we examine the derivative curve (Bourdarot, 1996) that shows three distinct flow phases as a function of time (Fig. 6). The first flow phase corresponds to the fracture flow (growing of the derivative), the second flow phase corresponds to a transition period during which matrix feeds the fracture (decay of the derivative), and the third flow phase corresponds to both fracture and matrix production.

Accordingly, the shape of the derivative observed on Fig. 4 might be characteristic of a dual porosity behavior. However, in the simulated fracture network the permeability and storativity of the matrix are not taken into account. So, if the shape of the derivative is related to a dual porosity behavior, we can assume that channels of low hydraulic conductivity provide the storage function (primary porosity) and that channels of high conductivity provide the transmissive function (secondary porosity). In this case, the 'V shape' of the derivative should vary as we change the conductivity contrast between the elements.

4.2. Effect of aperture contrast between elements on the hydrodynamic behavior

To understand the implications of a higher aperture (then conductivity) contrast between the various elements on the hydrodynamic behavior, we carried out two other simulations. For the first simulation (Fig. 7), the equivalent apertures of the channels were fixed at 0.001 and 0.003 m, respectively, which results in a conductivity ratio of 81 between the channels and yields the following hydraulic properties of the network:

$$\hat{K}_h = 1.7 \times 10^{-6}\ \mathrm{m\ s^{-1}};\ \hat{S}_s = 1.6 \times 10^{-6}\ \mathrm{m^{-1}};$$

$$\hat{D}_h = 1.06.$$

In the second simulation (Fig. 8), the equivalent apertures were fixed at 0.001 and 0.004 m, respectively, which results in a conductivity ratio of 256 between the channels and yields the following hydraulic properties:

$$\hat{K}_h = 3 \times 10^{-6}\ \mathrm{m\ s^{-1}};\ \hat{S}_s = 2.8\ 10^{-6}\ \mathrm{m^{-1}};$$

$$\hat{D}_h = 1.07.$$

For those two simulations, the increasing of the aperture contrast between the elements induces variations in the earlier hydrodynamic response, while the late time flow behavior is not affected. These changes in the earlier hydrodynamic flow response result in a 'dual porosity signature' that is as more accentuated as the aperture contrast increases.

In the synthetic networks, the volumetric density

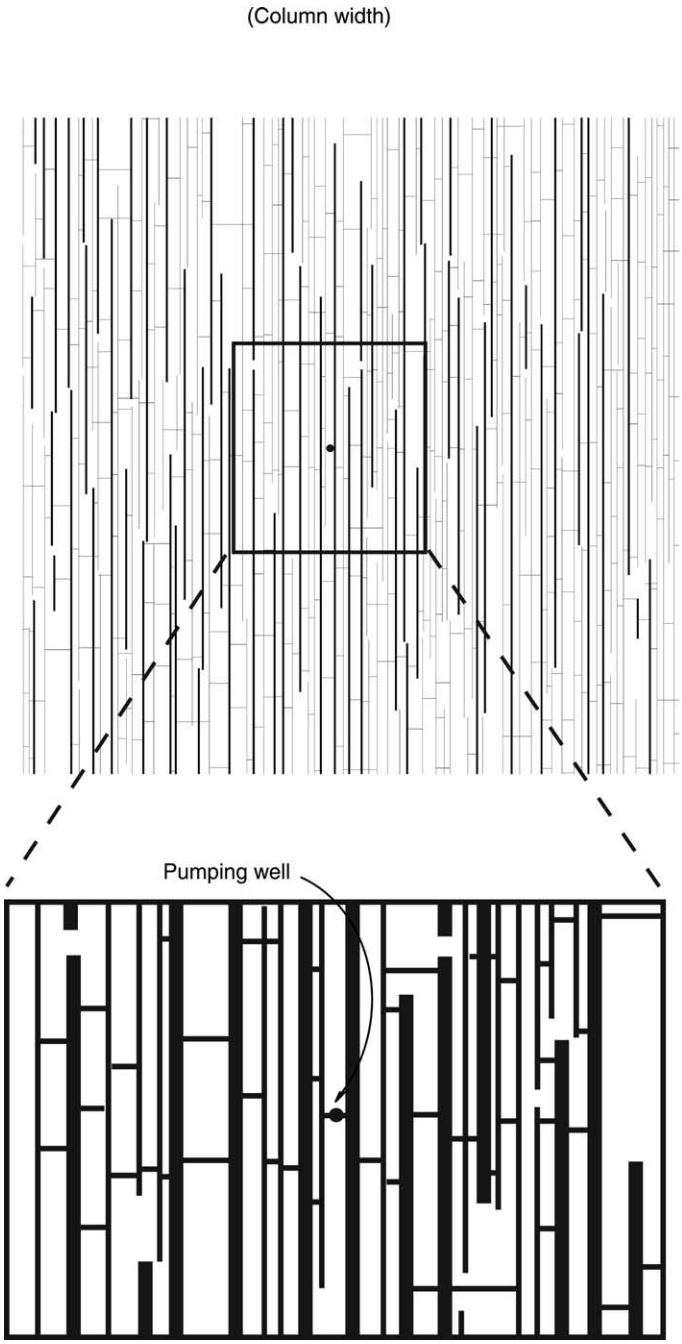

Fig. 5. Map view of bedding with simulated fracture sets. The pumping well intersects a low conductivity pipe of a second-generation fracture; this fracture is connected to a long and high fracture of first generation (on its right). Large aperture channels are represented by bold lines.

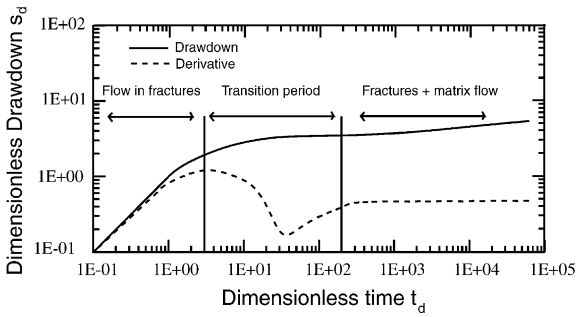

Fig. 6. Drawdown and derivative variations observed for a dual porosity behavior in a fracture aquifer (modified from Bourdarot (1996)).

[L/L^3] of, respectively, the high and low conductivity channels are of same order of magnitude. Thus, if we still assume that channels of low hydraulic conductivity provide the storage function (primary porosity) and that channels of high conductivity provide the transmissive function (secondary porosity), then a higher aperture contrast between the elements will generate a high transmissive function of the secondary porosity (K_f) and a low transmissive function of the primary porosity (K_m). Accordingly, this contrast should generate a more accentuated dual-porosity behavior. However, following the same hypothesis, the storage function of the primary porosity (S_m) will be lower than the storage function of the secondary porosity (S_f), which is in disagreement with the hypothesis required for a dual porosity behavior analysis.

Furthermore, the well is connected to the primary porosity (channel of low hydraulic conductivity), which differs from the assumptions usually considered for dual porosity model. Thus, this hydrodynamic behavior that looks like a dual porosity behavior, is related to another phenomenon since there are major discrepancies between the assumptions required for a dual porosity behavior and the well-aquifer properties of the simulated network.

In addition, if we consider the storativity ratio $\omega = S_f/(S_f + S_m)$ that relates the secondary (or fracture) storativity to that of the entire system, we observe that our system reacts in a different manner, as it should while considering a dual porosity model. Indeed, as the volumetric density of the high and low conductivity channels is of same order of magnitude, S_f and S_m are also of same order of magnitude for a low conductivity contrast if we keep assuming that channels of low conductivity correspond to the primary porosity and that channels of high conductivity correspond to the secondary porosity. In this case ω would be smaller for a low aperture contrast between channels (Fig. 4) than for a high aperture contrast (Figs. 7 and 8), since S_f becomes bigger than S_m. In a conventional dual porosity model, the 'V shape' of the derivative is as much accentuated, as ω parameter is low. Thus the 'V shape' observed on Fig. 4 should be more remarkable than on Fig. 7 that itself should be more accentuated than on Fig. 8. Instead the 'V shape' of the derivative is as much emphasized as ω parameter is high. In a same way, the beginning of the transition is as much later as ω is high in the case of a dual porosity model. In our case, we observe exactly the opposite (Figs. 4, 7 and 8). Thus, the variation of the hydrodynamic behavior with the ω parameter is opposite to what it should be according to

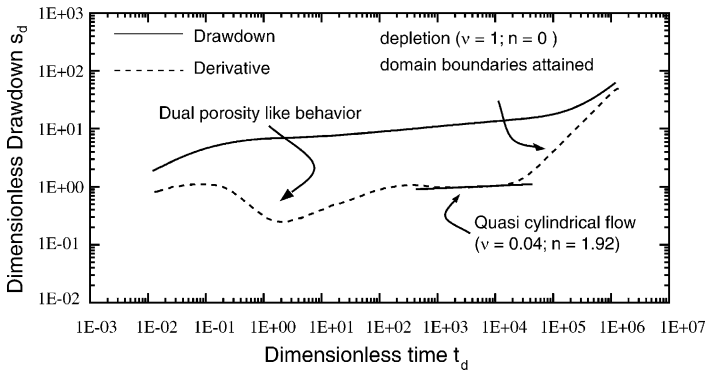

Fig. 7. Hydrodynamic response and transient-well-test signature on the pumping well when the equivalent apertures of the low and high conductivity pipes are, respectively, 0.001 and 0.003 m.

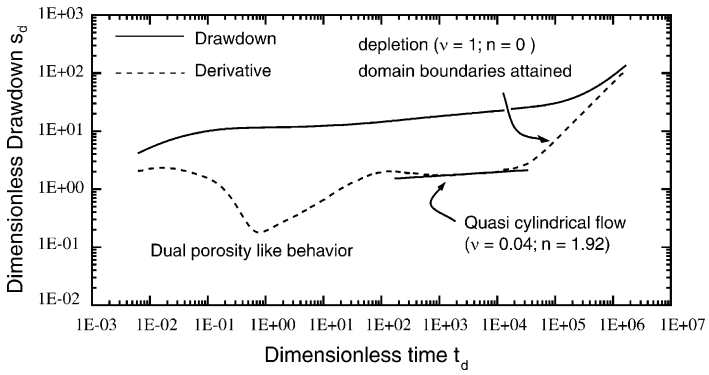

Fig. 8. Hydrodynamic response and transient-well-test signature on the pumping well when the equivalent apertures of the low and high conductivity pipes are, respectively, 0.001 and 0.004 m.

a dual porosity behavior, while considering that channels of low hydraulic conductivity provide the storage function (primary porosity) and that channels of high conductivity provide the transmissive function (secondary porosity). Note that the previous considerations induce another major contradiction with the usual dual porosity model assumption that implies $S_f \ll S_m$.

This shows that the first intuitive analysis of the hydrodynamic behavior is not appropriate and that this analysis might lead to the determination of inappropriate hydrodynamic parameters. Thus, we might be in a particular configuration where both high and low conductivity channels participate to the storage function of the system while the low conductivity channel linked to the well would provide the transmissive function towards the remainder of the aquifer.

4.3. Origin of the dual porosity-like behavior

In order to better understand the origin of the dual porosity-like behavior, we carried out other simulations on the same well, though this time by 'filtering' the network: The channels of low conductivity that do not affect network connectivity were removed in order to identify their contribution to the hydrodynamic response observed on the well. In this way, we check if they can provide the storage function of the network (primary porosity) and thus induce the 'dual porosity signature'.

Fig. 9 shows the hydrodynamic response on the well that intersects the same channel of low conductivity as for Fig. 8, with the same aperture contrast between the elements. We can observe that the dual porosity like behavior remains which, this time, is followed by a quasi-linear flow behavior ($n = 1.04$) related to the channels of high conductivity constitutive of first set fractures that control flow. Indeed, those high conductivity channels are mainly related to the first fracture set, thus they are more numerous with respect to the whole network than in the previous case, as most of the removed low conductivity channels are related to the second fracture set. As a consequence, the regional linear flow observed is due to the new connectivity of the network that now consists mainly of high conductivity channels whose direction is the one of first fracture set.

If the shape of the derivative were previously related to a dual porosity behavior, then the 'V' of the derivative should have been particularly attenuated because of the reduction of the storage function provided by the fractures of low conductivity (primary porosity). As the dual porosity like behavior remains, this demonstrates that high conductivity channels also participate to the storage function of the system. This highlights the major role of the connectivity in the vicinity of the well that is responsible for this dual porosity like flow behavior. Accordingly, the transient-well-test signature might be more the consequence of the connections between the well and the reservoir (channel of low conductivity) and to the presence of a large fracture in the vicinity of the well than to a storage function provided by the channels of low conductivity (primary porosity).

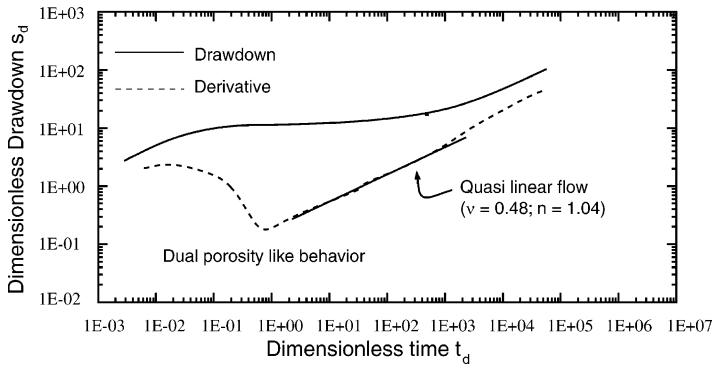

Fig. 9. Hydrodynamic response and transient-well-test signature on the pumping well when the pipes of low hydraulic conductivity that do not affect network connectivity are removed; the equivalent apertures of the low and high conductivity pipes are, respectively, 0.001 and 0.004 m.

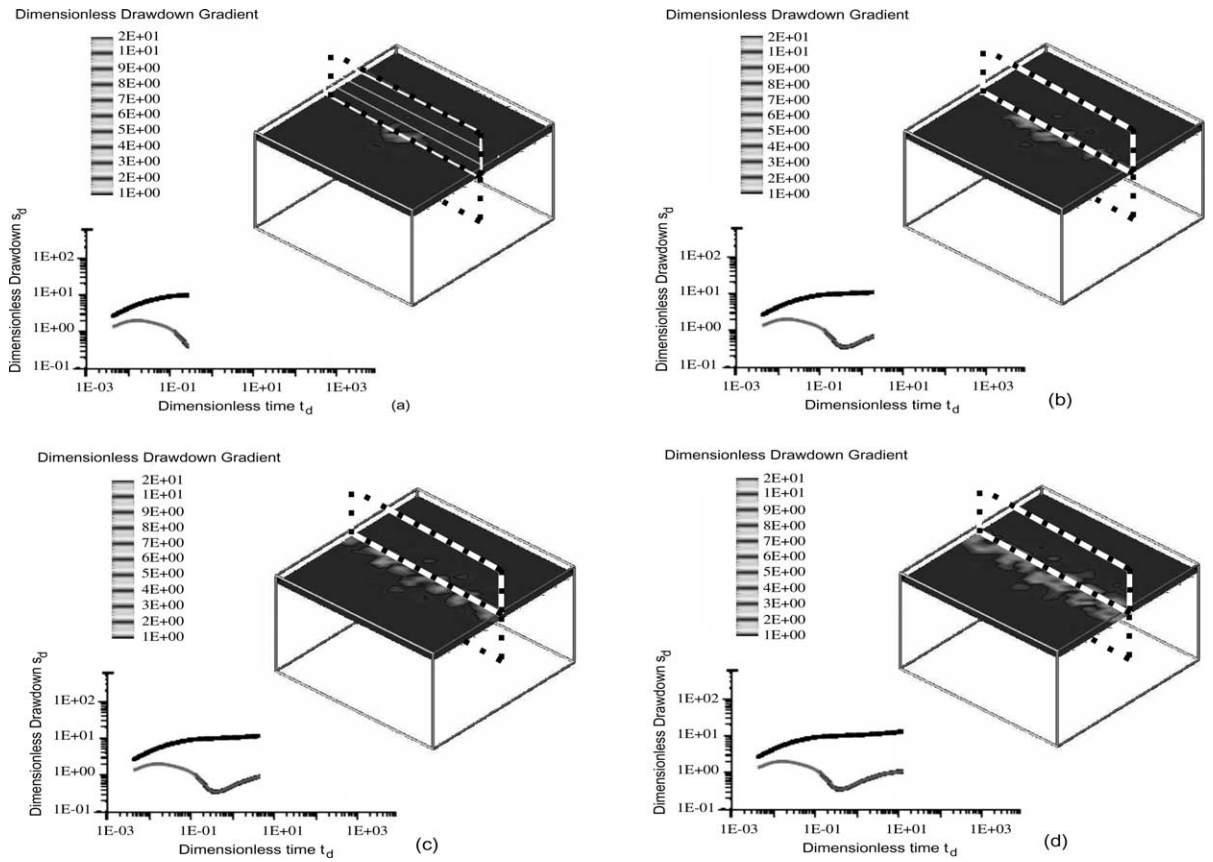

Fig. 10. Dimensionless fluid pressure propagation in the bedding parallel plane intersected by the well, hydrodynamic response and transient-well-test signature at the corresponding time. Interpolation of calculated drawdowns in pipes was used in order to visualize the signal propagation, assuming homogeneous parameters between fractures. The 'box' corresponds to the central part of the aquifer and has the same height and half the lateral size of the synthetic network. The long and high fracture in the vicinity of the well is schematically represented. (a) The pressure front encounters the large fracture, the derivative begins to fall; (b) the pressure front propagates in the large fracture whose storativity is solicited, the derivative drops; (c) the pressure front propagates around the strike of the large fracture that acts as a relay structure to fluid drainage, the derivative increases; (d) return to homogeneous behavior (the derivative corresponds almost to radial drawdown) with fluid drainage mostly controlled by the large fracture.

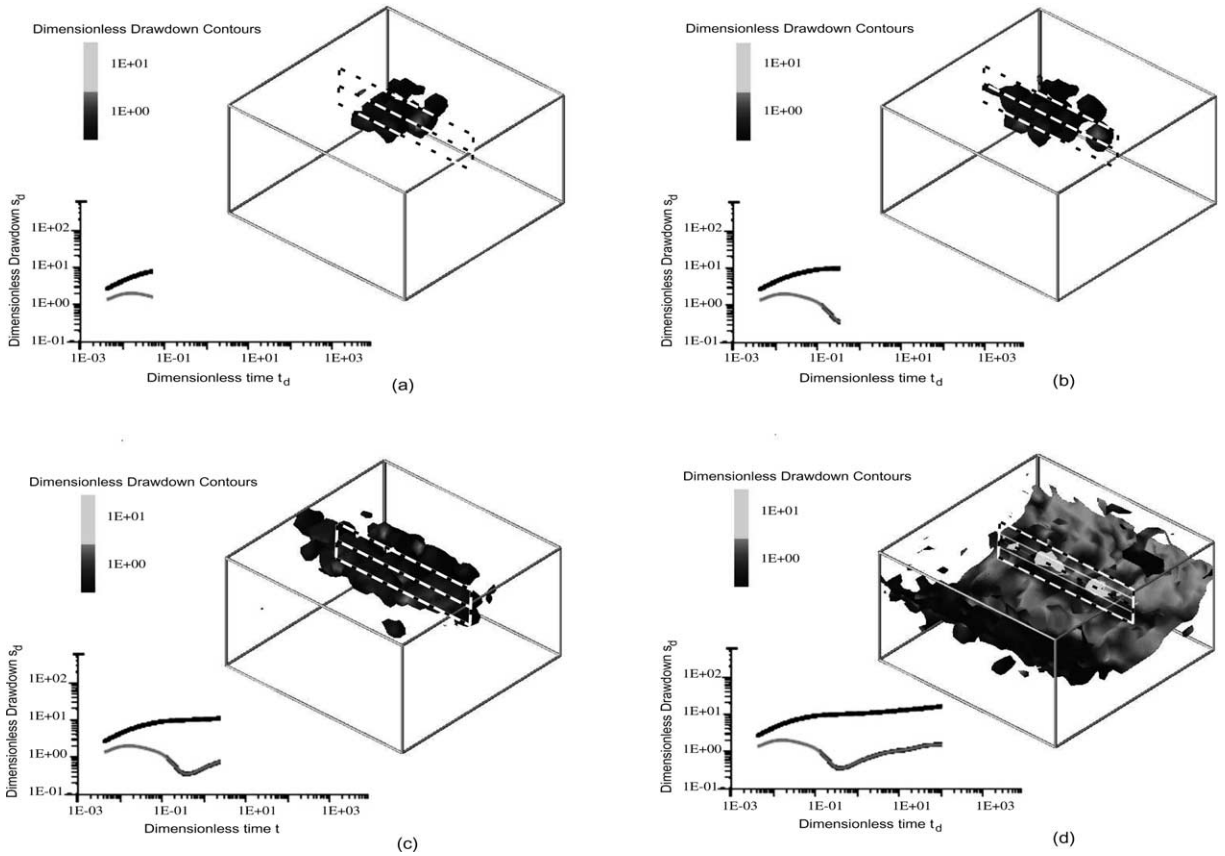

Fig. 11. Dimensionless fluid pressure propagation in the whole network, hydrodynamic response and transient-well-test signature at the corresponding time. Interpolation of calculated drawdowns in pipes was used in order to visualize the signal propagation, assuming homogeneous parameters between fractures. The represented domain is the same as for Fig. 10 and the large fracture is still schematized. (a) The pressure front encounters the large fracture, the derivative begins to fall; (b) the pressure front propagates in the large fracture whose storativity is solicited, the derivative drops; (c) the pressure front propagates around the strike of the large fracture that acts as a relay structure to fluid drainage, the derivative increases; (d) return to homogeneous behavior (the derivative corresponds almost to radial drawdown) with fluid drainage mostly controlled by the large fracture.

For a better understanding of the hydrodynamic behavior, we represented the propagation of pressure front as a function of time in the synthetic network (Figs. 10 and 11), for the simulation illustrated by Fig. 8. Fig. 10 shows the propagation, as a function of time, of isobaric contours (corresponding to pressure perturbation generated by the pumping test) within a bedding parallel plane comprising the channel intersected by the well (Fig. 5(a)). Fig. 11 shows the propagation in terms of time of isobaric surfaces within the whole network.

When the derivative begins to fall (Figs. 10(a) and 11(a)), the pressure perturbation front encounters a major fracture of the first set (schematized) constituted of high conductivity pipes (numerically determined). This fracture initially acts as a barrier to pressure perturbation propagation (Figs. 10(a) and 11(a)), then fills (the decrease in the derivative corresponds to the storage solicitation of pipes making up the fracture, Figs. 10(b) and 11(b)), thus permitting continued migration of the pressure perturbation into the remainder of the reservoir (Figs. 10(c) and 11(c)). Finally, the growth of the derivative curve corresponds to the return to a homogeneous flow behavior, nevertheless controlled by the fracture (Figs. 10(d) and 11(d)). Indeed, this high permeability fracture is under pressure relative to the remainder of the reservoir along its strike, such

that fluid at a large distance from the well first flows into the fracture's channels and then is focused towards the well. This results in a quasi-radial flow after the transient-well-test signature (Fig. 8) that corresponds to fluid drainage towards the large fracture and not towards the well.

Thus, the 'V shape' of the derivative that looks like a 'dual porosity signature' is related to a 'hydrodynamic barrier' to pressure propagation. This barrier corresponds to a large fracture that is composed of high conductivity channels and acts as a lateral heterogeneity.

We showed that in a fractured reservoir, a dual porosity signature may appear during the pressure transient response although we are in a configuration different from the hypothesis required for an analysis with a dual porosity model. Indeed, the well is connected to a low conductivity fracture (primary porosity) in our model, although it should be connected to a high conductivity fracture (secondary porosity) for a conventional analysis with a dual porosity model. Furthermore, we have shown that although we can interpret a pressure transient response in a fractured aquifer with a dual porosity model, this corresponds to a different phenomenon that is not in agreement with the dual porosity model hypothesis. Thus the interpretation will be erroneous and the parameters will not be characteristic of the system, which will induce errors in the estimation of reservoir parameters and thus in the management of the resources of the reservoir. This may also point out clearly the fact, that a dual-porosity like behavior can also be induced only by a complex fracture network itself.

5. Application to field data: dual porosity or lateral heterogeneity?

Fig. 12 corresponds to well test data in the Permian Pelite (Siliciclastic series) of Lodeve Basin (France). The fractured reservoir situated on this site (Fig. 13) is composed of two families of joints N10 ($\pm 10°$) and N100 ($\pm 10°$); the N10 fracture orientation corresponds to the longer joints associated with small subvertical faults oriented N20 ($\pm 10°$). The fracture apertures measured at the outcrop and in the subsurface are generally millimetric to centimetric (Bruel, 1997). Open channels developed in the bedding plane of the layers at intersections with fractures have been identified in mines (Bruel, 1997; Bruel et al., 1999). These authors showed that flow circulation preferentially occurs along the poorly tilted bedding planes at fracture (joint and small strike–slip faults) intersections, or at fracture–fracture intersection but also that flow is predominant along the N–S trend.

Bruel et al. (1999) have interpreted the well test data (Fig. 12) from this site with a dual porosity model (PIE software, Elf exploration production), while supposing that the well was intersecting a small fault of high conductivity at the proximity of the well (Bruel et al., 1999). They thus considered that the joint network provide the primary porosity and that the small fault provide the secondary porosity. Besides the ω and λ parameters previously described, PIE software uses the porosity Φ the horizontal permeability of the system k, and the skin that corresponds to a head loss (positive or negative) in the vicinity of the well. The spacing between the horizontal planes of the slab shaped blocks representative of the system has been estimated to be around 5 m, which corresponds to the average height of individual sedimentary units within the basin. Bruel et al. (1999) introduced an impervious barrier situated at 110 m from the well to explain the boundary effect observed on the well test data, which agrees with the compartmentalization of the reservoir between larger faults of E–W orientation. The well test data matched with the dual porosity model are reported on the graph (Fig. 12). This match was obtained with the following parameters: $\omega = 0.05$; $\lambda = 1.5 \times 10^{-7}$; skin $= -3.99$; $k = 5.32 \times 10^{-7}$ m s^{-1}; $\Phi = 0.25$.

This interpretation with a dual porosity model has been suggested by the presence of a small fault of high conductivity at the proximity of the well, while supposing that the well was intersecting it (Bruel et al., 1999). However, there is no evidence of the intersection between the fault and the well (Bruel, personal communication), which means that the observed dual porosity like hydrodynamic behavior could correspond to the previously described phenomenon, with a high conductivity fracture (the small fault) making up a lateral heterogeneity, as the configuration of the system well-aquifer is very close to the one of the previously studied synthetic network. The hydrodynamic response may therefore be related to the

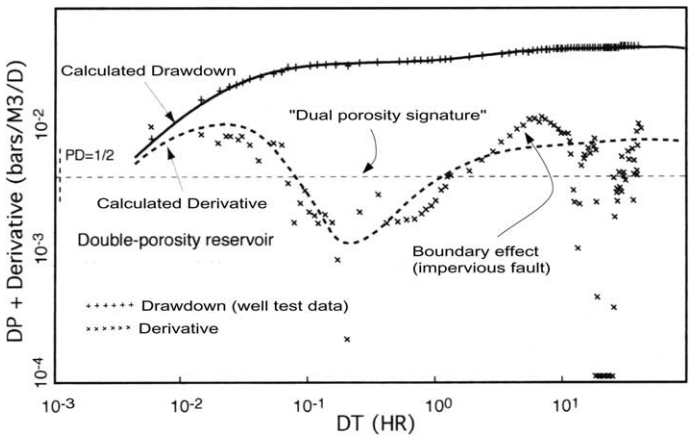

Fig. 12. Well test data of a well in proximity to a small fault of trend N15. Data have been interpreted with a dual porosity model (PIE), assuming that the well intersects the small fault and that the joint network assures the function storage.

connectivity in the surrounding of the well connected to the rest of the aquifer by a fracture of low conductivity linked to a high conductivity fracture (the small fault in this case).

Thus, our model might be able to reproduce the observed flow behavior, without considering a dual porosity behavior. On the field site, the dip is very low, so that the reservoir can be approximate by a tabular network; in addition, the 'useful flow network' consists of two sub-orthogonal fracture families and preferred flow paths are located at intersections between discontinuities. Accordingly, our model correctly matches the properties of the site that comprises two principal directions of fracturing with

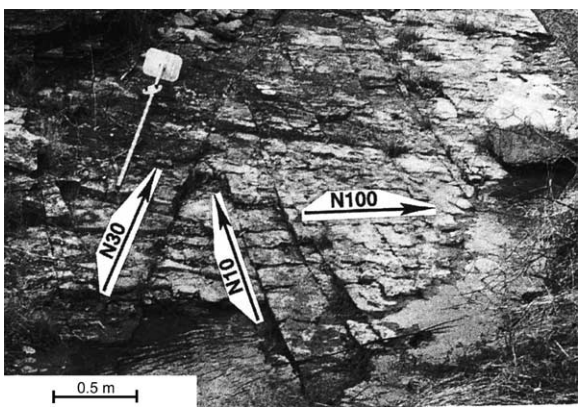

Fig. 13. Oblique view of the fractured aquifer constituted of Permian Pelite (siliciclastic series) found within the Lodeve basin of France, (photograph: T. Bruel).

flow located in channels at fracture intersections, which induces a hydraulic conductivity anisotropy related to the two families of fracture. As the normal offset of the strike–slip fault in the vicinity of the well is very small, we assume that it can be simulated by a large fracture with our joint network model.

The match obtained with the dual porosity model is obtained while using a dimensionless pressure (DP) although our model considers a dimensionless drawdown (s_d). Accordingly, we attempted to generate qualitatively and not quantitatively the same flow behavior. To do so, we ran a pumping test simulation in a synthetic network while considering the following hypothesis: the average thickness of the strata (th) has been fixed to 5 m and the average spacing between fractures was fixed to 50 cm, which is in accordance with field data (Bruel, 1997). To account for the previous horizontal permeability and porosity determined with the dual porosity model PIE to match the data, we chose a horizontal equivalent permeability $\hat{K}_h = 5 \times 10^{-7}\ \mathrm{m\ s^{-1}}$ and an equivalent specific storativity $\hat{S}_s = 2.5 \times 10^{-6}\ \mathrm{m^{-1}}$ (while considering $\hat{S}_s = \Phi\beta$ for the synthetic network. The negative skin introduced to match the data with the dual porosity model indicates an improvement in the flow near the wellbore, which happens when the well intersects one or many open channels or fractures.

Accordingly, in our model the well is located such as it intersects a channel of low conductivity and is in the proximity of the large fracture representative of the small fault. We chose this configuration as we

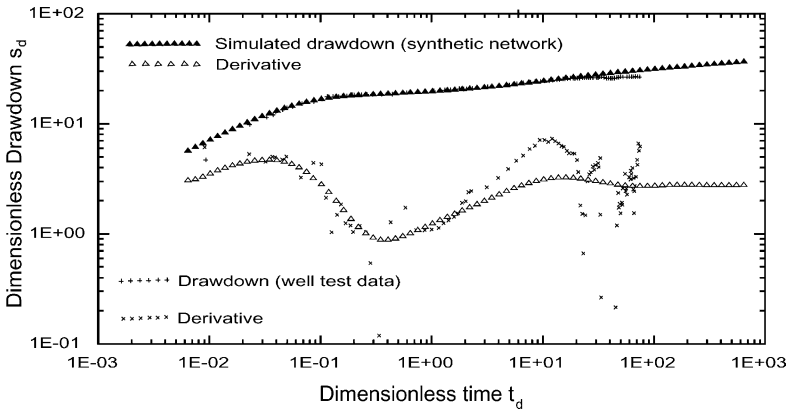

Fig. 14. Well-test data from the experimental site of Lodeve and simulated well-test data obtained from the synthetic network, with a vertical translation such as the qualitative match is better seen.

have shown that a lateral heterogeneity in proximity to the well (the small fault in this case) can induce a dual porosity like flow behavior.

The qualitative match of the well test data with our model (Fig. 14) is obtained when we consider a directional permeability ratio such as $K_y = 10 \times K_x$, with K_y and K_x, the equivalent permeability along the direction of the first generation (longer) joints and the second-generation joints, respectively. The plot of well test data and simulated data reported on a same graph with a vertical translation shows that the fit is qualitatively consistent (Fig. 14). Accordingly, the simulated transient-well-test signature related to a lateral heterogeneity, can qualitatively match the well test data.

Furthermore, the resulting equivalent aperture of the channels constitutive of the network calculated to obtain the previous hydrodynamic parameters, are, respectively, equal to 0.37 and 1.5 mm, which is consistent with field data (Bruel, 1997) that gave a measured aperture lower than millimetric for the joints and millimetric to centimetric for the fault. We thus qualitatively explained the same flow behavior with our model while being consistent with field data, showing that the use of a dual porosity model is not necessarily appropriate. Instead, this is the connectivity in the vicinity of the well that may induce this dual porosity like behavior, which can simply result from the presence of a high conductivity small fault making up a lateral heterogeneity.

6. Summary and conclusions

The focus of this study was to determine what confidence can be given to the transient-well-test signature when pumping is carried out on a unique wellbore and how a well known flow behavior like dual porosity can wrongly be used to interpret a hydrodynamic response related to a different phenomenon. We thus propose an alternative deterministic interpretation with another type of model that incorporates fracture interactions and conductivity anisotropy.

In this paper, we showed how the flow behavior is affected by changing the hydrodynamic properties of channels constitutive of the dual fracture network and by modifying its connectivity. We thus observed that the earlier hydrodynamic response is strongly controlled by the aperture contrast between the flow paths as well as by the connectivity in the vicinity of the well. The representation, in terms of time, of the propagation of isobaric surfaces during a simulated pumping test revealed that flow characteristics that may be interpreted as a dual porosity flow behavior are in fact related to a lateral heterogeneity (large fracture or small fault). We saw that a large fracture near the well first acts as a 'hydrodynamic barrier' to pressure propagation then as a relay structure to drainage since remote fluid first flows in its channels and then is focused toward the well. Thus the observed dual porosity like transient-well-test signature is different of the classical dual porosity behavior

for which it is considered that flow first occurs within fractures that afterwards are fed by the matrix.

We thus showed that when a dual porosity model matches well test data, the resulting reservoir parameters can be erroneous because of the model assumptions basis that are not necessarily verified. Accordingly a model, like the dual porosity model, intended to explain complex natural phenomenon must be used very cautiously. Indeed, the misuse of a model to interpret well test data can lead to incorrect analysis. That is why the flow behavior must correctly be identified in order to determine the hydrodynamic properties since it is a very important factor in the strategy not only for the management of an aquifer or an oil reservoir, but also for the rehabilitation of a polluted aquifer.

With a field example where the fractured reservoir comprises such lateral heterogeneity, we have shown that well test data obtained on this site could also be related to the connectivity and the presence of a small fault in the surrounding of the well. Indeed, our model was found to correctly match the properties of the experimental site, both from a geometric and hydrodynamic point of view. We thus showed that the connectivity in the area immediately surrounding the pumping well is very important in controlling the flow and efficient exploitation of this type of fractured reservoir. These results also indicate that the consideration of fracture interaction mechanisms during network generation, which allows the representation of the structure of natural dual fracture networks, is of great importance since the connectivity that exerts a strong effect on flow behavior is correctly simulated.

Well test data from a single well must therefore be used cautiously to assess the flow properties of fractured reservoirs with lateral heterogeneities such as large fractures or small faults. It will often be necessary to consider test responses from multiple wells to unambiguously determine the hydrodynamic properties of the fractured reservoirs, in such a configuration of the pumping well within the aquifer.

Acknowledgements

The authors wish to thank the F.L. Paillet and J.C. Roegiers for their helpful comments and suggestions, as well as S. Böttcher for its review of the translation. The Centre National Universitaire Sud de Calcul (CNUSC) of Montpellier (France) provided free access to powerful tools for simulation processes and 3D visualization (P. Falandry).

References

Bai, T., Gross, M.R., 1999. Theoretical analysis of cross-joint geometries and their classification. J. Geophys. Res. 104 (B1), 1163–1177.

Barker, J.A., 1988. A generalized radial flow model for hydraulic tests in fractured rock. Water Resour. Res. 24 (10), 1796–1804.

Barker, J.A., 1991. The reciprocity principle and an analytical solution for Darcian flow in network. Water Resour. Res. 27 (5), 743–746.

Barthélémy, P., Jacquin, C., Yao, J., Thovert, J.F., Adler, P.M., 1996. Hierarchical structures and hydraulic properties of fracture network in the Causse of Larzac. J. Hydrol. 187, 237–258.

Becker, A., Gross, M.R., 1996. Mechanism for joint saturation in mechanically layered rocks: an example from southern Israel. Tectonophysics 257, 233–237.

Bourdarot, G., 1996. Essais de puits: méthodes d'interprétation, Editions Technip, Paris, p. 352.

Bourdet, D., Ayoub, J.A., Whittle, T.M., Pirard, Y.M., Kniazeff, V., 1983. Interpretating well tests in fractured reservoirs. World Oil 1975, 77–87.

Bruel, T., 1997. Caractérisation des circulations de fluides dans un réseau fracturé et rôle des contraintes in situ, PhD Thesis (in french), Thèse de l'Université Montpellier II, p. 402.

Bruel, T., Petit, J.P., Massonnat, G., Guerin, R., Nolf, J.L., 1999. Relation entre écoulements et fractures ouvertes dans un système aquifère compartimenté par des failles et mise en évidence d'une double porosité de fractures. Bull. Soc. Geol. France 170 (3), 401–412.

Cacas, M.C., Ledoux, E., De Marsily, G., Tillie, B., 1990. Modeling fracture flow with a stochastic discrete fracture network: calibration and validation-1/the flow model. Water Resour. Res. 26 (3), 479–489.

Cornaton, F., Perrochet, P., 2002. Analytical 1-D dual-porosity equivalent solutions to 3-D discrete single-continuum models. Application to karstic spring hydrograph modeling. J. Hydrol. 262, 164–175.

Domenico, P., Schwartz, F.W., 1990. Physical and Chemical Hydrogeology, Wiley, New York, p. 824.

Drogue, C., Grillot, J.C., 1976. Structure géologique et premières observations piézometriques à la limite du sous système karstique de Terrieu. Géologie 3 (25).

Drogue, C., Costa Almeida, C.A., 1984. Déformations cassantes et structure de magasin dans la couverture carbonatée mésozoïque du centre du Portugal (Est du plateau de Fatima). C.R. Acad. Sci. 299(II) (9), 577–580.

Ezzedine, S., 1994. Modélisation des écoulements et du transport dans les milieux fissurés. Approches continue et discontinue,

PhD Thesis, Thèse de l'Ecole Nationale Supérieure des Mines de Paris, p. 208.

Gringarten, A.C., Ramey, H.J., Raghavan, R., 1974. Unsteady state pressure distributions created by a well with a horizontal fracture, partial penetration, or restricted entry. SPE J., 413–426.

Hamm, S.Y., Bidaux, P., 1996. Dual-Porosity fractal models for transient flow analysis in fissured rocks. Water Resour. Res. 32, 2733–2745.

Hobbs, D.W., 1967. The formation of tension joints in sedimentary rocks: an explanation. Geol. Mag. 104, 550–556.

Horne, R.N., 1995. Modern Well Test Analysis: a Computer-Aided Approach, Petroway Inc, Palo Alto, CA, p. 185.

Huang, Q., Angelier, J., 1989. Fracture spacing and its relation to bed thickness. Geol. Mag. 126 (4), 355–362.

Jourde, H., 1999. Simulation d'essais de puits en milieu fracturé à partir d'un modèle discret basé sur les lois mécaniques de fracturation. Validation sur sites expérimentaux, PhD Thesis, Mémoires Géosciences Montpellier, 11, p. 205.

Jourde, H., Bidaux, P., Pistre, S., 1998. Modélisation des écoulements en réseaux de fractures orthogonales: influence de la localisation du puits de pompage sur les rabattements. Bull. Soc. Geol. France 169 (5), 635–644.

Pollard, D.D., Aydin, A., 1988. Progress in understanding jointing over the past century. Geol. Soc. Am. Bull. 100, 1181–1204.

Price, N.J., Cosgrove, J.W., 1990. Analysis of Geological Structures, Cambridge University Press, Cambridge.

Rives, T., Rawnsley, K., Petit, J.P., 1994. Analogue simulation of orthogonal joint set formation in brittle varnish. J. Struct. Geol. 16 (3), 419–429.

Sanderson, D.J., Zhang, X., 1997. Modeling and prediction of localized flow in fractured rock-masses. AAPG Bull. 81 (8), 1409–1410.

Segall, P., Pollard, D.D., 1983. Joint formation in granitic rock of the Sierra Nevada. Geol. Soc. Am. Bull. 94, 563–575.

Stehfest, H., 1970. Commun. ACM 13, 47–49.

Theis, C.V., 1935. The relation between the lowering of the piezometric surface and the rate and duration of discharge of a well using groundwater storage. AGU, 16th Annu. Meet., 519–524.

Warren, J.E., Root, P.J., 1963. The behavior of naturally fractured reservoirs. SPE J. 3 (2), 245–255.

Wu, H., Pollard, D.D., 1995. An experimental study of the relationship between joint spacing and layer thickness. J. Struct. Geol. 17 (6), 887–905.